Dynamic modeling and flight control of a balloon-quadcopter unmanned aerial vehicle

Davi Antonio Santos, Americo Cunha Jr

DYNAMIC MODELING AND FLIGHT CONTROL OF A BALLOON-QUADCOPTER UNMANNED AERIAL VEHICLE

Davi Antnio dos Santos

davists@ita.br

Aeronautics Institute of Technology

Praa Mal. Eduardo Gomes, 50, 12228-900, São José dos Campos, SP, Brazil

Americo Cunha Jr

americo@ime.uerj.br

Rio de Janeiro State University

Rua São Francisco Xavier, 524, 20550-900, Rio de Janeiro, RJ, Brazil

Abstract. *The present work is concerned with the dynamic modeling as well as the design of position and attitude control laws for a balloon-multirotor vehicle consisting of an oblate spheroid helium balloon coupled with a quadrotor airframe. A six-degrees-of-freedom nonlinear dynamic model is derived for the balloon-quadcopter using the Newton-Euler approach. To capture the contact flexibility between the balloon and the airframe, the center of buoyancy is supposed to oscillate with second-order dynamics with respect to the airframe. Under the assumption of time-scale separation between the translational and rotational dynamics, the attitude and position control laws are designed separately from each other. Both the attitude and position control laws are proportional-derivative actions plus feedforward compensation of nonlinearities combined with control input saturation within appropriate parallelepipedal sets. These constraint sets are carefully chosen in order to satisfy torque and force design bounds. Computer simulation is carried out to assess the performance of the proposed balloon-quadcopter control system under nominal conditions.*

Keywords: *multirotor aerial vehicle, flight control, balloon-multicopter, balloon-quadcopter.*

1 INTRODUCTION

In the last few years, the multirotor aerial vehicles (MAVs) have found many applications, including small package delivering, precise agriculture monitoring, surveillance in urban areas, building inspections, just to cite a few. In most cases, the operation could become more effective and efficient if the flight duration and payload capacity were extended. A straightforward way to improve the payload capacity and flight duration of a multirotor aerial vehicle is by combining it with a balloon filled with a lifting gas, such as helium or hydrogen. The balloon provides a net aerostatic lift that is oriented contrary to the vehicle weight, thus reducing the equivalent load supported by the multirotor airframe. In general, we name such a combination as a balloon-multicopter. In particular, the present paper is concerned with a small balloon-quadcopter with a diameter of 1.8 m, whose payload capacity is of 0.5 kg. Besides the aforementioned advantages of the new aerial vehicle over the MAVs, one can also highlight its simplicity compared to other vehicles with good payload and flight duration capabilities, such as the blimps and the conventional fuel-engine helicopters. The former has a more complex construction that includes vectoring rotors and aerodynamic surfaces (Khoury and Gillet, 1999), while the latter requires elaborated mechanical linkages and a swashplate (Leishman, 2006).

The design of a control system for a balloon-multicopter, even if it is intended to operate indoors with low speed, presents a critical challenge due to the restoring torque generated by the displacement of the balloon's center of buoyancy (CB) above the vehicle's center of mass (CM). For a fixed CB-CM displacement, the larger the inclination angle of the vehicle with respect to the local vertical, the larger the magnitude of the restoring torque. Therefore, for a given design of the rotor set, the attitude controller must respect a maximum bound on the inclination angle for the control system to maintain its effectiveness. The side effect of this constraint is usually a low lateral acceleration capability.

It is worth pointing out that there is no literature yet available on flight dynamics and control of a balloon-multicopter. Therefore, we base our derivations and methods on the well-known and popular literature on MAVs as well as on basic aerostatic fundamentals (namely, on Archimedes' Principle). The reference Bertrand et al. (2011) details the design of a flight control system for MAVs based on the time-scale separation assumption between the attitude dynamics (which is the faster one) and the position dynamics (which is slower). From this assumption, one can split the flight control design into two derivations: one for the attitude control law and the other one for the position control law. Both control laws provide virtual actuation variables that must be converted into commands to the real effectors of the vehicle via control allocation (Johansen and Fossen, 2013). There are a plenty of methods for designing attitude and position controllers for MAVs, using different control strategies such as saturated-PD controllers (Santos et al., 2013), model predictive controllers (Prado and Santos, 2017), and sliding model controllers (Silva and Santos, 2016), just to cite a few examples.

The present paper is specifically concerned with the dynamic modeling and design of flight control laws for a small balloon-quadcopter. A nonlinear six-DOF dynamic model is derived for the vehicle using the Newton-Euler approach. Besides the efforts to which the conventional MAVs are usually subject, the proposed model includes the restoring torque due to the displacement of the balloon's CB above the vehicle's CM. Based on the time-scale separation assumption, the flight control system is structured in a hierarchical architecture, in which the attitude control is realized by an inner loop while the position control is carried out by an outer loop.

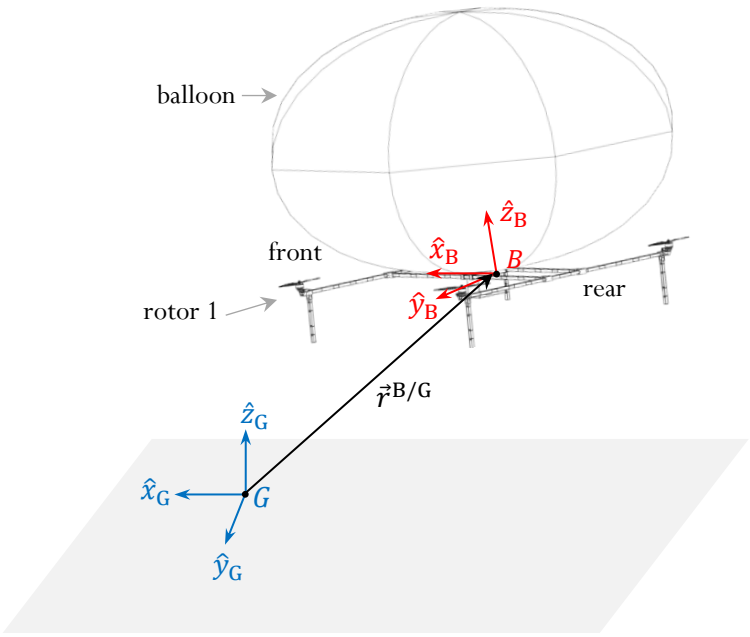

Figure 1: The Cartesian coordinate systems (CCS). $S_B = \{\hat{x}_B, \hat{y}_B, \hat{z}_B\}$ is the body CCS and $S_G = \{\hat{x}_G, \hat{y}_G, \hat{z}_G\}$ is the ground CCS.

The attitude and position control laws are separately designed using proportional-derivative controllers with feedforward compensation of nonlinearities and considering the saturation of the control vector within appropriate parallelepipedal sets that ensure the satisfaction of design bounds on the control torque and force.

The remaining text is organized as follows. Section 2 derives a six-DOF dynamic model for the balloon-quadcopter. Section 3 is concerned with the design of the nonlinear attitude and position control laws as well as the control allocations. Section 4 evaluates the proposed control system in a nominal scenario using computer simulation. Finally, Section 5 conclude's the paper.

2 DYNAMIC MODELING

This section derives the rotational and translational equations of motion and actuator models for the balloon-quadcopter under consideration. We start with preliminary definitions in Subsection 2.1, then we model the rotor dynamics and control efforts in Subsection 2.2, the restoring torque and aerostatic lift generated by the balloon in Subsection 2.3, the vehicle's rotational dynamics in Subsection 2.4, and its translational dynamics in Subsection 2.5.

2.1 Preliminary Definitions

We define two Cartesian coordinate systems (CCS), as illustrated in Figure 1. The body CCS, $S_B \triangleq \{\hat{x}_B, \hat{y}_B, \hat{z}_B\}$ is attached to the vehicle's body with the origin at the vehicle's center of mass B, the $\hat{x}_B$ axis pointing forward, the $\hat{z}_B$ axis pointing upward, normal to the rotor plane, and the $\hat{y}_B$ axis completing a right-handed coordinate system. The ground CCS, $S_G \triangleq \{\hat{x}_G, \hat{y}_G, \hat{z}_G\}$ is fixed to the ground at a known point G, with the $\hat{z}_G$ axis pointing upward vertically. For our purposes, S_G can be considered as an inertial frame.

The notation adopted here distinguishes between two kinds of vectors: physical vectors and algebraic vectors. Physical vectors are denoted by lowercase italic letters with a right arrow superscript, *e.g.*, $\vec{r}$. The corresponding algebraic vector, resulting from the projection of $\vec{r}$ onto an arbitrary CCS S_{A} is denoted by a lowercase boldface letter with the subscript A, *i.e.*, $\mathbf{r}_{\mathrm{A}} \in \mathbb{R}^3$. The text will often refer to $\mathbf{r}_{\mathrm{A}}$ as the S_{A} representation of $\vec{r}$. Now consider a relative vector physical quantity $\vec{a}$ (such as position or velocity) of the CCS S_{A} with respect to another CCS S_{B}. In this case, we would better explicitly denote this physical vector by $\vec{a}^{\mathrm{A/B}}$ and its S_{A} and S_{B} representations by $\mathbf{a}_{\mathrm{A}}^{\mathrm{A/B}}$ and $\mathbf{a}_{\mathrm{B}}^{\mathrm{A/B}}$, respectively. The attitude of S_{A} w.r.t. S_{B} is fundamentally represented by the attitude matrix $\mathbf{D}^{\mathrm{A/B}} \in \mathrm{SO}(3)$; consider the physical vector $\vec{r}$ and its representations $\mathbf{r}_{\mathrm{A}}$ and $\mathbf{r}_{\mathrm{B}}$. The attitude matrix $\mathbf{D}^{\mathrm{A/B}}$ is such that $\mathbf{r}_{\mathrm{A}} = \mathbf{D}^{\mathrm{A/B}}\mathbf{r}_{\mathrm{B}}$.

Consider two algebraic vectors $\mathbf{a} = [a_1 \ a_2 \ a_3]^{\mathrm{T}}$ and $\mathbf{b}$. We denote the vector product between them by the matrix multiplication $[\mathbf{a}\times]\mathbf{b}$, where $[\mathbf{a}\times]$ is a skew-symmetric matrix

$$[\mathbf{a}\times] \triangleq \begin{bmatrix} 0 & -a_3 & a_2 \\ a_3 & 0 & -a_1 \\ -a_2 & a_1 & 0 \end{bmatrix}. \tag{1}$$

2.2 Rotor Dynamics and Efforts

The set of four rotors equipping the airframe is responsible for generating the control forces and torques as described here. The ith rotor individually produces a thrust force and a reaction torque on the airframe along the $\hat{z}_{\mathrm{B}}$ axis with magnitudes denoted by f_i and τ_i, respectively. We describe these efforts by the following aerodynamic models:

$$f_i = k_f \omega_i^2, \tag{2}$$

$$\tau_i = k_\tau \omega_i^2, \tag{3}$$

$i = 1, ..., 4$, where k_f is the thrust force coefficient, k_τ is the reaction torque coefficient, and ω_i is the rotation speed of the ith rotor. The rotor dynamics can be modeled by the following first-order linear model:

$$\dot{\omega}_i = -\frac{1}{\tau_\omega}\omega_i + \frac{k_\omega}{\tau_\omega}\bar{\omega}_i, \tag{4}$$

where $\bar{\omega}_i \in [0, \bar{\omega}_{\max}]$ is the rotation speed command of the ith rotor, k_ω is the speed coefficient, and τ_ω is the rotor time constant. The rotation bound $\bar{\omega}_{\max}$ is assumed to be known.

Consider that all the four thrusts f_i point upward. Moreover, consider that the reaction torque τ_1 is positive, τ_2 is negative, τ_3 is positive, and τ_4 is negative. Figure 1 identifies rotor 1 and the other ones are labeled sequentially in the clockwise direction. Therefore, one can show that the magnitude F^c of the resulting control force and the S_{B} representation $\mathbf{T}_{\mathrm{B}}^c$ of the resulting control torque are given by

$$\begin{bmatrix} F^c \\ \mathbf{T}_{\mathrm{B}}^c \end{bmatrix} = \mathbf{\Gamma}\mathbf{f}, \tag{5}$$

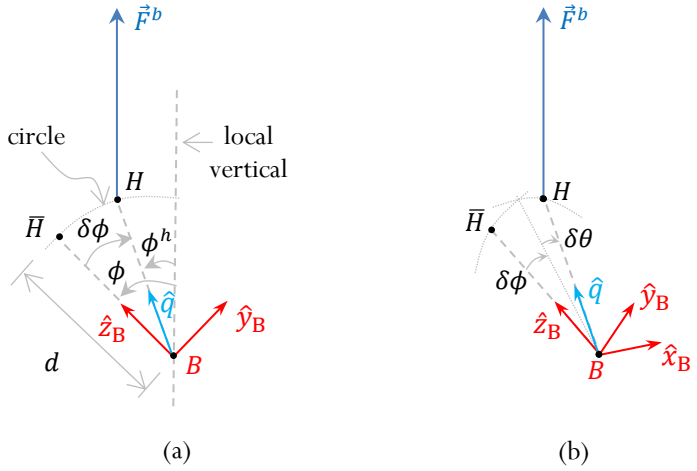

Figure 2: The restoring torque and contact flexibility. (a) two-dimensional view. (b) three-dimensional view.

where $\mathbf{f} \triangleq [f_1 \ f_2 \ f_3 \ f_4]^{\mathrm{T}}$ and

$$\mathbf{\Gamma} \triangleq \begin{bmatrix} 1 & 1 & 1 & 1 \\ l & -l & -l & l \\ -l & -l & l & l \\ k & -k & k & -k \end{bmatrix} \in \mathbb{R}^{4\times 4}, \tag{6}$$

where l is the length of each vehicle's arm with respect to CM, and $k \triangleq k_\tau/k_f$.

2.3 Aerostatic Lift and Restoring Torque

This subsection models two crucial efforts generated by the balloon. One is an aerostatic lift force $\vec{F}^b$ and the other one is a restoring torque $\vec{T}^b$. The force $\vec{F}^b$ is explained by the Archimedes' Principle, which says that it always points upwards parallel to the local vertical and its magnitude is equal to the weight of the air volume displaced by the balloon minus the weight of the lifting gas (the helium) itself. Therefore, one can immediately write the S_{G} representation of $\vec{F}^b$ as

$$\mathbf{F}^b_{\mathrm{G}} = \begin{bmatrix} 0 \\ 0 \\ Vg(\rho_{\mathrm{air}} - \rho_{\mathrm{helium}}) \end{bmatrix}, \tag{7}$$

where V is the volume of the balloon, g is the gravitational acceleration, ρ_{air} is the air density, and ρ_{helium} is the helium density.

On the other hand, the restoring torque $\vec{T}^b$ is an effort acting about the vehicle's CM, which appears as a consequence of the displacement d between the balloon's CB and the vehicle's

CM. Figure 2 depicts a physical model for the connection between the airframe and the balloon, which is assumed here to be flexible. The CB effective position is at point H. The most relevant effect of this flexibility is in the motion of H w.r.t. S_{B}, which in turn causes an oscillation in $\mathbf{T}_{\mathrm{B}}^{b}$. In this case, the restoring torque can be written as

$$\vec{T}^{b} = (d\hat{q}) \times \vec{F}^{b}, \tag{8}$$

where $\hat{q}$ is the unit vector pointing from the center of mass B to the actual position H of the center of buoyancy. Representing equation (8) in S_{B}, we thus have

$$\mathbf{T}_{\mathrm{B}}^{b} = [(d\mathbf{q}_{\mathrm{B}})\times]\mathbf{D}^{\mathrm{B/G}} \begin{bmatrix} 0 \\ 0 \\ F^{b} \end{bmatrix}, \tag{9}$$

where $\mathbf{q}_{\mathrm{B}} = [\sin\delta\theta \;\; \sin\delta\phi \;\; \cos\delta\phi\cos\delta\theta]^{\mathrm{T}}$, $\delta\phi \triangleq \phi^{h} - \phi$, $\delta\theta \triangleq \theta^{h} - \theta$, ϕ and θ are the roll and pitch angles corresponding to $\mathbf{D}^{\mathrm{B/G}}$, and ϕ^{h} and θ^{h} are the roll and pitch angles representing the attitude of $\hat{q}$ w.r.t. S_{G}. In order to acquire both the elasticity and the damping of the balloon-airframe connection, ϕ^{h} and θ^{h} are modeled as 2nd order followers of ϕ and θ, respectively, *i.e.*,

$$\ddot{\phi}^{h} + K^{d}\dot{\phi}^{h} + K^{s}\phi^{h} = K^{s}\phi, \tag{10}$$

$$\ddot{\theta}^{h} + K^{d}\dot{\theta}^{h} + K^{s}\theta^{h} = K^{s}\theta, \tag{11}$$

where K^{d} is a damping coefficient and K^{s} is a stiffness coefficient.

2.4 Rotational Motion

The kinematics equation of the rotational motion of S_{B} w.r.t. S_{G} is given in $\mathrm{SO}(3)$ by

$$\dot{\mathbf{D}}^{\mathrm{B/G}} = -\left[\mathbf{\Omega}_{\mathrm{B}}^{\mathrm{B/G}}\times\right]\mathbf{D}^{\mathrm{B/G}}, \tag{12}$$

where $\mathbf{\Omega}_{\mathrm{B}}^{\mathrm{B/G}}$ is the S_{B} representation of the vehicle's angular velocity w.r.t. S_{G}.

Assume that the vehicle has a rigid structure and S_{G} is an inertial frame. Therefore, the Second Euler's Law yields

$$\dot{\mathbf{H}}_{\mathrm{B}} + \left[\mathbf{\Omega}_{\mathrm{B}}^{\mathrm{B/G}}\times\right]\mathbf{H}_{\mathrm{B}} = \mathbf{T}_{\mathrm{B}}^{c} + \mathbf{T}_{\mathrm{B}}^{b} + \mathbf{T}_{\mathrm{B}}^{d}, \tag{13}$$

where $\mathbf{H}_{\mathrm{B}}$ is the S_{B} representation of the total angular momentum of the vehicle, $\mathbf{T}_{\mathrm{B}}^{c}$ is the S_{B} representation of the control torque (see equation (5)), $\mathbf{T}_{\mathrm{B}}^{d}$ is the S_{B} representation of the (unknown) disturbance torque, and $\mathbf{T}_{\mathrm{B}}^{b}$ is the S_{B} representation of the balloon restoring torque (see Subsection 2.3).

Considering the rotation of both the body and the propellers and noting that the latter rotates much faster, the total angular momentum $\mathbf{H}_{\mathrm{B}}$ can be written in the form

$$\mathbf{H}_{\mathrm{B}} = \mathbf{J}^{b}\mathbf{\Omega}_{\mathrm{B}}^{\mathrm{B/G}} + J^{r}\sum_{i=1}^{4}(-1)^{i}\omega_{i}\mathbf{e}_{3}, \tag{14}$$

where $\mathbf{J}^b \in \mathbb{R}^{3\times3}$ is the inertia matrix of the vehicle and $J^r \in \mathbb{R}$ is the moment of inertia of the rotors about $\hat{z}_{\mathrm{B}}$.

Therefore, by replacing equation (14) into equation (13), one can obtain the dynamic equation of the rotational motion of S_{B} w.r.t. S_{G} with vectors represented in S_{B}:

$$\begin{aligned}\dot{\mathbf{\Omega}}_{\mathrm{B}}^{\mathrm{B/G}} = \left(\mathbf{J}^b\right)^{-1} \left[\left(\mathbf{J}^b \mathbf{\Omega}_{\mathrm{B}}^{\mathrm{B/G}} + J^r \sum_{i=1}^{4} (-1)^i \omega_i \mathbf{e}_3 \right) \times \right] \mathbf{\Omega}_{\mathrm{B}}^{\mathrm{B/G}} \\ - \left(\mathbf{J}^b\right)^{-1} \left(J^r \sum_{i=1}^{4} (-1)^i \dot{\omega}_i \mathbf{e}_3 + \mathbf{T}_{\mathrm{B}}^b + \mathbf{T}_{\mathrm{B}}^c + \mathbf{T}_{\mathrm{B}}^d \right).\end{aligned} \tag{15}$$

2.5 Translational Motion

By invoking the Second Newton's Law considering all the vectors represented in S_{G}, one can immediately write

$$\mathbf{M}\ddot{\mathbf{r}}_{\mathrm{G}}^{\mathrm{B/G}} = \mathbf{F}_{\mathrm{G}}^g + \mathbf{F}_{\mathrm{G}}^b + \mathbf{F}_{\mathrm{G}}^c + \mathbf{F}_{\mathrm{G}}^d, \tag{16}$$

$$\mathbf{M} \triangleq m^t \mathbf{I}_3 + \begin{bmatrix} m^h \mathbf{I}_2 & \mathbf{0}_{2\times1} \\ \mathbf{0}_{1\times2} & 0 \end{bmatrix}, \tag{17}$$

where m^t is the total mass of the vehicle without lifting gas and including the payload, $m^h = \rho_{\mathrm{helium}} V$ is the helium mass, $\mathbf{r}_{\mathrm{G}}^{\mathrm{B/G}} \in \mathbb{R}^3$ is the S_{G} representation of the position of the vehicle's center of mass B w.r.t. G, $\mathbf{F}_{\mathrm{G}}^g$ is the S_{G} representation of the gravitational force, $\mathbf{F}_{\mathrm{G}}^b$ is the S_{G} representation of the balloon aerostatic lift force, $\mathbf{F}_{\mathrm{G}}^c$ is the S_{G} representation of the control force, and $\mathbf{F}_{\mathrm{G}}^d$ is the S_{G} representation of the (unknown) disturbance force. The force $\mathbf{F}_{\mathrm{G}}^b$ is given by equation (7), while $\mathbf{F}_{\mathrm{G}}^g$ and $\mathbf{F}_{\mathrm{G}}^c$ are modeled by

$$\mathbf{F}_{\mathrm{G}}^g = \begin{bmatrix} 0 \\ 0 \\ -m^t g \end{bmatrix} \quad \text{and} \quad \mathbf{F}_{\mathrm{G}}^c = \left(\mathbf{D}^{\mathrm{B/G}}\right)^{\mathrm{T}} \begin{bmatrix} 0 \\ 0 \\ F^c \end{bmatrix}. \tag{18}$$

By replacing equations (17)-(18) into (16), we finally obtain the dynamic model for the translational motion

$$\ddot{\mathbf{r}}_{\mathrm{G}}^{\mathrm{B/G}} = F^c \mathbf{M}^{-1} \mathbf{n}_{\mathrm{G}} + \begin{bmatrix} 0 \\ 0 \\ Vg(\rho_{\mathrm{air}} - \rho_{\mathrm{helium}})/m^t - g \end{bmatrix} + \mathbf{M}^{-1} \mathbf{F}_{\mathrm{G}}^d, \tag{19}$$

where $\mathbf{n}_{\mathrm{G}} \in \mathbb{R}^3$ is the transpose of the third line of $\mathbf{D}^{\mathrm{B/G}}$, which corresponds to the S_{G} representation of the unit vector normal to the rotor plane.

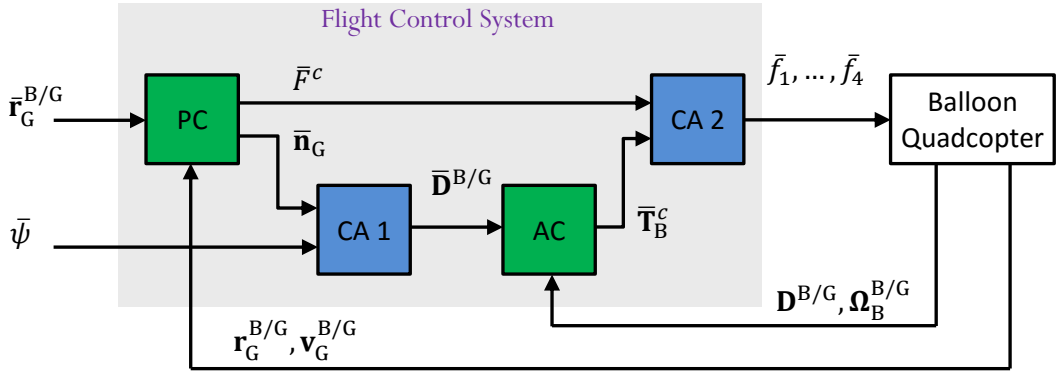

Figure 3: Architecture of the balloon-quadcopter control system. PC: position controller; AC: attitude controller; CA 1, CA 2: control allocations.

3 FLIGHT CONTROL SYSTEM

A hierarchical control strategy is adopted here, as illustrated in Figure 3. In this strategy, the flight control is realized by two nested control loops, where the inner loop is responsible for the attitude control, while the outer loop performs position control. The position controller receives an external position command $\bar{\mathbf{r}}_{\mathrm{G}}^{\mathrm{B/G}}$ as well as feedbacks of position $\mathbf{r}_{\mathrm{G}}^{\mathrm{B/G}}$ and velocity $\mathbf{v}_{\mathrm{G}}^{\mathrm{B/G}}$ from the vehicle. On the other hand, it produces the thrust command vector $\bar{F}^c\bar{\mathbf{n}}_{\mathrm{G}}$. The force command direction $\bar{\mathbf{n}}_{\mathrm{G}}$ together with an external heading command $\bar{\psi}$ are processed in the control allocation block CA 1 to provide the three-DOF attitude command $\bar{\mathbf{D}}^{\mathrm{B/G}}$. The attitude controller receives feedback of the vehicle's three-dimensional attitude $\mathbf{D}^{\mathrm{B/G}}$ and angular velocity $\boldsymbol{\Omega}_{\mathrm{B}}^{\mathrm{B/G}}$. Finally, the control allocation block CA 2 is responsible for generating the individual thrust commands $\bar{f}_i$, $i = 1, ..., 4$, from the total thrust magnitude command $\bar{F}^c$ and torque command $\bar{\mathbf{T}}_{\mathrm{B}}^c$.

3.1 Time-Scale Separation

The control architecture of Figure 3 is the classical and ubiquitous one in the MAV control literature. It is based on the assumption that there is a time-scale separation between the closed-loop translational and rotational vehicle dynamics Bertrand et al. (2011). This assumption is ensured by tuning the attitude control loop to converge much faster then the position control loop. Under such conditions, when designing the position control law, one can assume that the actual attitude $\mathbf{D}^{\mathrm{B/G}}$ converges to the corresponding command $\bar{\mathbf{D}}^{\mathrm{B/G}}$ instantaneously. In other words, one can assume $\mathbf{D}^{\mathrm{B/G}} = \bar{\mathbf{D}}^{\mathrm{B/G}}$. On the other hand, when designing the attitude control law, the attitude command $\bar{\mathbf{D}}^{\mathrm{B/G}}$ is assumed to be constant, or equivalently, the angular velocity command $\bar{\boldsymbol{\Omega}}_{\mathrm{B}}^{\mathrm{B/G}}$ is assumed to be zero. On the basis of these assumptions, the attitude and position control laws can be designed separately as detailed in the sequel.

3.2 Attitude Control

The design model adopted for deriving the attitude control law is obtained from equation (15) by: 1) neglecting the disturbance torque, 2) replacing the actual control torque $\mathbf{T}_{\mathrm{B}}^c$ by

the corresponding command $\bar{\mathbf{T}}_{\mathrm{B}}^{c}$, 3) considering that the rotor dynamics is so fast that one can assume $\dot{\omega}_i = 0$ and $\omega_i = \bar{\omega}_i$, and 4) the balloon-airframe connection is rigid. The resulting design model is

$$\dot{\boldsymbol{\Omega}}_{\mathrm{B}}^{\mathrm{B/G}} = \left(\mathbf{J}^{b}\right)^{-1} \left[\left(\mathbf{J}^{b}\boldsymbol{\Omega}_{\mathrm{B}}^{\mathrm{B/G}} + J^{r} \sum_{i=1}^{4} (-1)^{i} \bar{\omega}_i \mathbf{e}_3 \right) \times \right] \boldsymbol{\Omega}_{\mathrm{B}}^{\mathrm{B/G}} - F^{b} \left(\mathbf{J}^{b}\right)^{-1} [(d\mathbf{e}_3)\times] \mathbf{D}^{\mathrm{B/G}} \mathbf{e}_3 + \left(\mathbf{J}^{b}\right)^{-1} \bar{\mathbf{T}}_{\mathrm{B}}^{c}. \tag{20}$$

Suppose that the torque command $\bar{\mathbf{T}}_{\mathrm{B}}^{c}$ is bounded from $-\mathbf{T}^{\max} \in \mathbb{R}^3$ to $\mathbf{T}^{\max} \triangleq [T_1^{\max}\, T_2^{\max}\, T_3^{\max}]^{\mathrm{T}}$. On the basis of the above design model, we propose the following attitude controller:

$$\bar{\mathbf{T}}_{\mathrm{B}}^{c} = \boldsymbol{\sigma}_{[-\mathbf{T}^{\max}, \mathbf{T}^{\max}]}(\boldsymbol{\gamma}^{a}), \tag{21}$$

where $\boldsymbol{\gamma}^{a} \triangleq [\gamma_1^a\, \gamma_2^a\, \gamma_3^a]^{\mathrm{T}} \in \mathbb{R}^3$ is defined by

$$\boldsymbol{\gamma}^{a} \triangleq - F^{b}[(d\mathbf{e}_3)\times]\mathbf{D}^{\mathrm{B/G}}\mathbf{e}_3 + \left[\boldsymbol{\Omega}_{\mathrm{B}}^{\mathrm{B/G}}\times\right] \mathbf{J}^{b}\boldsymbol{\Omega}_{\mathrm{B}}^{\mathrm{B/G}} + J^{r} \left[\boldsymbol{\Omega}_{\mathrm{B}}^{\mathrm{B/G}}\times\right] \mathbf{e}_3 \sum_{i=1}^{4} (-1)^{i} \bar{\omega}_i + \mathbf{J}^{b}\mathbf{K}_1\boldsymbol{\varepsilon} - \mathbf{J}^{b}\mathbf{K}_2\boldsymbol{\Omega}_{\mathrm{B}}^{\mathrm{B/G}}, \tag{22}$$

where $\boldsymbol{\varepsilon} \in \mathbb{R}^3$ are the Euler angles (1-2-3 sequence) corresponding to the attitude control error $\tilde{\mathbf{D}} = \bar{\mathbf{D}}^{\mathrm{B/G}}(\mathbf{D}^{\mathrm{B/G}})^{\mathrm{T}}$, $\mathbf{K}_1, \mathbf{K}_2 \in \mathbb{R}^{3\times 3}$ are the controller gains, and

$$\boldsymbol{\sigma}_{[-\mathbf{T}^{\max}, \mathbf{T}^{\max}]}(\boldsymbol{\gamma}^{a}) \triangleq \begin{bmatrix} \sigma_{[-T_1^{\max}, T_1^{\max}]}(\gamma_1^a) \\ \sigma_{[-T_2^{\max}, T_2^{\max}]}(\gamma_2^a) \\ \sigma_{[-T_3^{\max}, T_3^{\max}]}(\gamma_3^a) \end{bmatrix}, \tag{23}$$

$$\sigma_{[-T_l^{\max}, T_l^{\max}]}(\gamma_l^a) \triangleq \begin{cases} -T_l^{\max}, & \gamma_l^a < -T_l^{\max} \\ \gamma_l^a, & \gamma_l^a \in [-T_l^{\max}, T_l^{\max}] \\ T_l^{\max}, & \gamma_l^a > T_l^{\max} \end{cases}, \; l = 1, 2, 3. \tag{24}$$

Note that the proposed attitude control law (21)-(22) is such that, if no saturation is active, it cancels out the first and second term on the right-hand side of equation (20), remaining a feedback-linearized dynamics controlled by the proportional-derivative actions appearing in the last two terms of equation (22).

3.3 Position Control

Here, the design model is obtain from equation (19), by assuming that: 1) the disturbance force $\mathbf{F}_{\mathrm{G}}^{d}$ is negligible, 2) the actual control force magnitude F^{c} is identical to the corresponding command $\bar{F}^{c}$, and 3) $\mathbf{D}^{\mathrm{B/G}} = \bar{\mathbf{D}}^{\mathrm{B/G}}$ (time-scale separation). The resulting design model is

$$\ddot{\mathbf{r}}_{\mathrm{G}}^{\mathrm{B/G}} = \mathbf{M}^{-1}\bar{\mathbf{F}}_{\mathrm{G}}^{c} + \begin{bmatrix} 0 \\ 0 \\ Vg(\rho_{\mathrm{air}} - \rho_{\mathrm{helium}})/m^{t} - g \end{bmatrix}, \tag{25}$$

where $\bar{\mathbf{F}}_{\mathrm{G}}^{c} = \bar{F}^{c}\bar{\mathbf{n}}_{\mathrm{G}} \in \mathbb{R}^3$ is the control force command and $\bar{\mathbf{n}}_{\mathrm{G}} \in \mathbb{R}^3$ is its direction vector, or equivalentely, the transpose of the third line of $\bar{\mathbf{D}}^{\mathrm{B/G}}$.

Suppose that $\bar{\mathbf{F}}_{\mathrm{G}}^{c}$ is bounded within a parallelepipedal set from $\mathbf{F}^{\min} \triangleq [F_1^{\min}\ F_2^{\min}\ F_3^{\min}]^{\mathrm{T}} \in \mathbb{R}^3$ to $\mathbf{F}^{\max} \triangleq [F_1^{\max}\ F_2^{\max}\ F_3^{\max}]^{\mathrm{T}} \in \mathbb{R}^3$. On the basis of the above design model, we propose the following position controller:

$$\bar{\mathbf{F}}_{\mathrm{G}}^{c} = \boldsymbol{\sigma}_{[\mathbf{F}^{\min},\mathbf{F}^{\max}]}(\boldsymbol{\gamma}^{p}), \tag{26}$$

where

$$\boldsymbol{\gamma}^{p} \triangleq -\begin{bmatrix} 0 \\ 0 \\ Vg(\rho_{\mathrm{air}} - \rho_{\mathrm{helium}}) - m^{t}g \end{bmatrix} + \mathbf{M}\mathbf{K}_3\left(\bar{\mathbf{r}}_{\mathrm{G}}^{\mathrm{B/G}} - \mathbf{r}_{\mathrm{G}}^{\mathrm{B/G}}\right) - \mathbf{M}\mathbf{K}_4\dot{\mathbf{r}}_{\mathrm{G}}^{\mathrm{B/G}} \tag{27}$$

and the saturation function $\boldsymbol{\sigma}_{[\mathbf{F}^{\min},\mathbf{F}^{\max}]}(.)$ is as defined in equations (23)-(24). The matrices $\mathbf{K}_3, \mathbf{K}_4 \in \mathbb{R}^{3\times3}$ are the controller gains.

Note that, similar to the attitude controller, the proposed position controller (26)-(27) is such that, if no saturation is active, it cancels out the second term on the right-hand side of equation (25), remaining a double-integrator dynamics controlled by the proportional-derivative actions appearing in the last two terms of equation (27). In saturation-free conditions, it is straightforward to show asymptotic stability of the proposed translational control loop using linear time-invariant control methods.

3.4 Control Allocation

Let us start with the control allocation CA 1. It provides the attitude command $\bar{\mathbf{D}}^{\mathrm{B/G}}$ from the two-DOF attitude represented by $\bar{\mathbf{n}}_{\mathrm{G}}$ and the external heading command $\bar{\psi}$. One can express the three-DOF attitude command $\bar{\mathbf{D}}^{\mathrm{B/G}}$ in terms of the corresponding Euler angles $\bar{\phi}$, $\bar{\theta}$, and $\bar{\psi}$ in the 1-2-3 sequence (Markley and Crassidis, 2014):

$$\bar{\mathbf{D}}^{\mathrm{B/G}} = \begin{bmatrix} \mathrm{c}\bar{\psi}\mathrm{c}\bar{\theta} & \mathrm{c}\bar{\psi}\mathrm{s}\bar{\theta}\mathrm{s}\bar{\phi} + \mathrm{s}\bar{\psi}\mathrm{c}\bar{\phi} & -\mathrm{c}\bar{\psi}\mathrm{s}\bar{\theta}\mathrm{c}\bar{\phi} + \mathrm{s}\bar{\psi}\mathrm{s}\bar{\phi} \\ -\mathrm{s}\bar{\psi}\mathrm{c}\bar{\theta} & -\mathrm{s}\bar{\psi}\mathrm{s}\bar{\theta}\mathrm{s}\bar{\phi} + \mathrm{c}\bar{\psi}\mathrm{c}\bar{\phi} & \mathrm{s}\bar{\psi}\mathrm{s}\bar{\theta}\mathrm{c}\bar{\phi} + \mathrm{c}\bar{\psi}\mathrm{s}\bar{\phi} \\ \mathrm{s}\bar{\theta} & -\mathrm{c}\bar{\theta}\mathrm{s}\bar{\phi} & \mathrm{c}\bar{\theta}\mathrm{c}\bar{\phi} \end{bmatrix}. \tag{28}$$

To specify $\bar{\phi}$ and $\bar{\theta}$, one can just compare the third line of (28) with the transpose of $\bar{\mathbf{n}}_{\mathrm{G}} \triangleq [\bar{n}_1\ \bar{n}_2\ \bar{n}_3]^{\mathrm{T}}$, to obtain $\bar{\phi} = -\tan^{-1}\bar{n}_2/\bar{n}_3$ and $\bar{\theta} = \sin^{-1}\bar{n}_1$.

Now, let us look at the control allocation CA 2. Equation (5) related the true resultant efforts F^c and $\mathbf{T}_{\mathrm{B}}^{c}$ with the four individual thrust forces compacted in $\mathbf{f} \in \mathbb{R}^4$. One can induce that the respective effort commands $\bar{F}^c$ and $\bar{\mathbf{T}}_{\mathrm{B}}^{c}$ are interrelated by

$$\begin{bmatrix} \bar{F}^{c} \\ \bar{\mathbf{T}}_{\mathrm{B}}^{c} \end{bmatrix} = \boldsymbol{\Gamma}\bar{\mathbf{f}}, \tag{29}$$

where $\bar{\mathbf{f}} \triangleq \left[\bar{f}_1\ \bar{f}_2\ \bar{f}_3\ \bar{f}_4\right]^{\mathrm{T}}$ and $\mathbf{\Gamma} \in \mathbb{R}^{4\times4}$ is given in (6). One can verify that $\mathbf{\Gamma}$ is non-singular and, therefore, the control allocation of the block CA 2 has a unique solution that is immediately obtained by inverting equation (29), *i.e.*,

$$\bar{\mathbf{f}} = \mathbf{\Gamma}^{-1} \begin{bmatrix} \bar{F}^c \\ \\ \bar{\mathbf{T}}^c_{\mathrm{B}} \end{bmatrix}. \tag{30}$$

4 SIMULATION-BASED EVALUATION

This section presents the results of a deterministic simulation of the proposed flight control system under nominal conditions. Subsection 4.1 describes the simulation and shows the adopted nominal parameters, while Subsection 4.2 presents and analyzes the simulation results.

4.1 Plant and Controller Parameters

For simulating the overall closed-loop flight control system illustrated in Figure 3, we use the models formulated in Section 2 as well as the control laws and control allocations proposed in Section 3. Table 1 shows the values of the balloon-quadcopter parameters that we assume to be deterministic in the present study. On the other hand, Table 2 presents the adopted controller parameters. The controller gains are tuned by trial and error, taking into account their proportional or derivative effect and considering the time-scale separation assumption as well.

Table 1: Deterministic parameters of the plant.

Description	Symbol	Value
Force coefficient	k_f	1.2838×10^{-5} N/(rad/s)^2
Torque coefficient	k_τ	3.0811×10^{-7} Nm/(rad/s)^2
Maximum rotor speed	$\bar{\omega}_{\max}$	906.66 rad/s
Motor speed coefficient	k_ω	1
Motor time constant	τ_ω	0.01 s
Arm length	l	0.9 m
Volume of the balloon	V	2.4 m^3
CB-CM displacement	d	0.76 m
Total inertia matrix	$\mathbf{J}^b$	$\mathrm{diag}(0.1, 0.1, 0.2)$ Kgm^2
Moment of inertia of the rotors	J^r	0.005 Kgm^2
Total empty mass	m^t	3.5 Kg
Damping parameter	K^d	25.1
Stiffness parameter	K^s	157.9

Table 2: Parameters of the attitude and position control laws.

Description	Symbol	Value
Proportional gain of the attitude controller	$\mathbf{K}_1$	$\mathrm{diag}(200, 200, 200)$
Derivative gain of the attitude controller	$\mathbf{K}_2$	$\mathrm{diag}(50, 50, 50)$
Proportional gain of the position controller	$\mathbf{K}_3$	$\mathrm{diag}(0.4, 0.4, 0.4)$
Derivative gain of the position controller	$\mathbf{K}_4$	$\mathrm{diag}(1, 1, 1)$
Maximum torque command	$\mathbf{T}^{\max}$	$[\ 8.34 \quad 8.34 \quad 0.22\ ]^{\mathrm{T}}$ Nm
Minimum force command	$\mathbf{F}^{\min}$	$[\ -4.67 \quad -4.67 \quad 1.03\ ]^{\mathrm{T}}$ N
Maximum force command	$\mathbf{F}^{\max}$	$[\ 4.67 \quad 4.67 \quad 20.6\ ]^{\mathrm{T}}$ N
Maximum inclination angle	$\varphi^{\max}$	24.4 degrees

In this paper, for obtaining simulation data that are consistent with a typical operation of MAVs, the proposed flight control system is commanded to follow a waypoint-based position trajectory. In this trajectory, the waypoints are connected by straight lines with length of 5 m and constant desired velocity of $\bar{v} = 0.5$ m/s. Moreover, the heading angle command $\bar{\psi}$ is set to zero.

4.2 Deterministic Simulation Results

Figures 4–7 are the results of the deterministic simulation using the parameters of Table 1–2. Figure 4 shows the effective position and the corresponding position command. In the ramp part of the component trajectories, one can verify a steady-state error of about 1.2 m. After finishing the ramp commands, the overshoot and accommodation time (of 5 cm around the final value) are approximately 3 mm and 4 s, respectively.

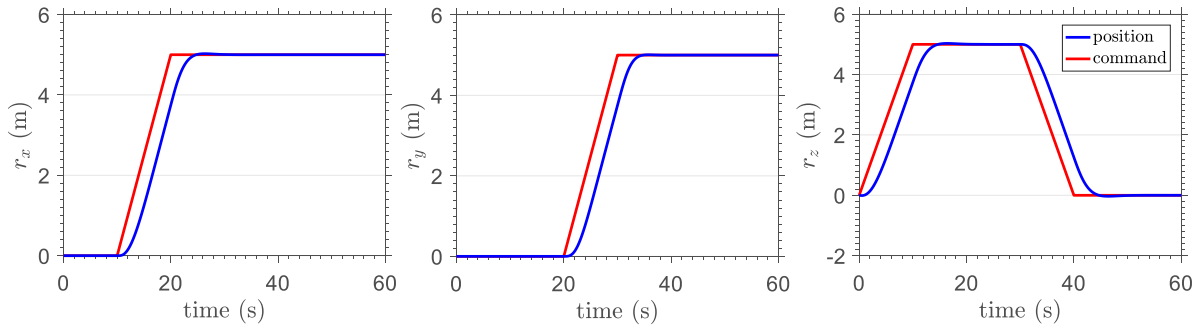

Figure 4: Deterministic performance of the position control.

Figure 5 shows the performance of the attitude control loop. First, one can see that the roll and pitch commands generated from the output of the position controller are smooth and smaller than 4 degrees. Moreover, the effective roll and pitch angles track the respective commands with very small error. The last graphic shows a negligible transient in the yaw angle at about 20 s, with a peak value of 0.0054 deg, when the vehicle starts to move horizontally.

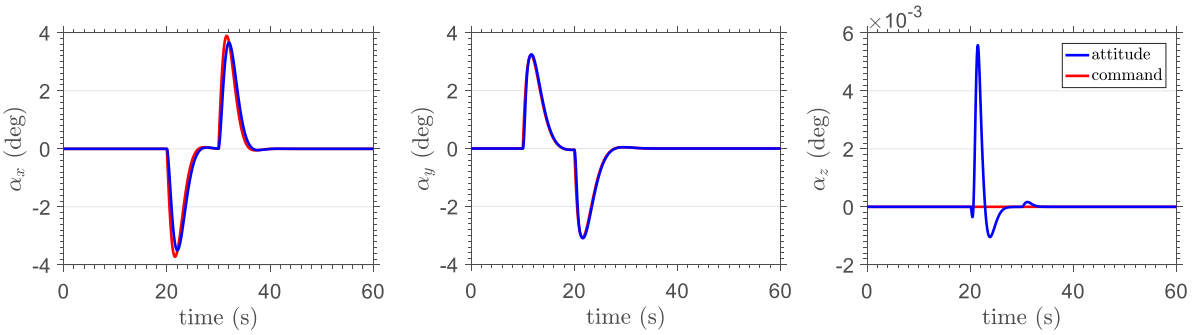

Figure 5: Deterministic performance of the attitude control.

Figure 6 shows the components of the torque command $\bar{\mathbf{T}}_{\mathrm{B}}^{c}$ produced by the attitude controller and Figure 7 presents the components of the force command $\bar{\mathbf{F}}_{\mathrm{G}}^{c}$ computed by the position controller. The force commands do not reach their maximum bounds, even at the beginning part of the trajectory, from 0 to 10 s, when the vehicle is commanded to ascend. After the transients caused by the maneuvers at the waypoints, $\bar{F}_z$ seems to converge and stay around the equivalent weight 30.3 N of the balloon-quadcopter, which is equal to the total weight of the vehicle and payload minus the aerostatic lift. On the other hand, $\bar{F}_x$ and $\bar{F}_y$ tend to converge to zero. During all the simulation, the components of $\bar{\mathbf{T}}_{\mathrm{B}}^{c}$ keep inside their bounds $\pm\mathbf{T}^{\max}$ with a large margin.

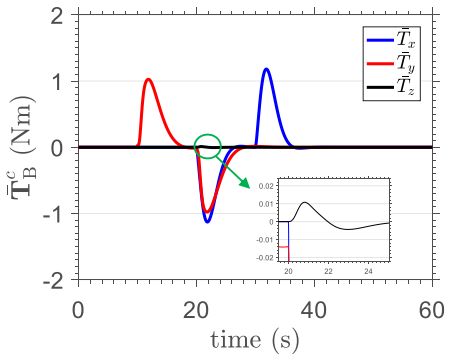

Figure 6: Torque command in the deterministic simulation.

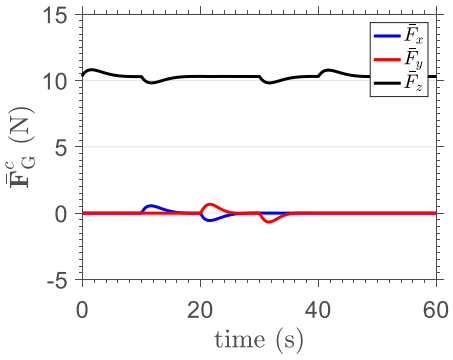

Figure 7: Force magnitude command in the deterministic simulation.

5 Conclusions

The paper proposed a flight control system for a new multirotor aerial vehicle (MAV) resulting from the combination of a quadcopter airframe with a balloon filled with helium. This MAV is a straightforward attempt to extend the flight duration and load capacity of conventional multirotor vehicles by means of an aerostatic lift. On one hand, such a combination results in a very simple vehicle. On the other hand, even for indoor flight, its control system must be carefully designed to overcome the effects of a restoring torque (which does not occur in conventional MAVs).

The proposed flight control system is evaluated on the basis of a deterministic simulation, which shows that in nominal conditions, it is possible to control the vehicle's position to follow a desired waypoint-based trajectory with a slow reference speed of 0.5 m/s. The obtained performance is sufficient accurate and fast for many MAV applications.

For future works, we will quantify the effects of the uncertainties in the wind conditions as well as in the flexible connection between the balloon and the airframe.

ACKNOWLEDGEMENTS

The authors would like to thank all those people who indirectly contributed or motivated us to conduct the present investigation. In special, we are grateful to Mr. Luciano S. Araujo (from Elio Tecnologia), who designed and built a balloon-hexacopter and donated it to the Laboratório de Robótica Area of the Aeronautics Institute of Technology (ITA). The financial supports of the Brazilian agencies FAPESP, FAPERJ, CNPq, and CAPES are also highly appreciated.

REFERENCES

Bertrand, S., Gunard, N., Hamel, T. Piet-Lahanier, H., Eck, L. A Hierarchical Controller for Miniature VTOL UAVs: Design and Stability Analysis Using Singular Perturbation Theory, *Control Engineering Practice*, 19 (10), 2011, 1099-1108.

Johansen, T. A., Fossen, T. I. Control Allocation - A Survey, *Automatica*, 46, 2013, 1087-1103.

Khoury, G. A., Gillet, J. D. (ed) *Airship Technology*. Cambridge University Press, 1999.

Leishman, J. G. *Principles of Helicopter Aerodynamics*. Cambridge University Press, 2006.

Markley, F. L., Crassidis, J. L. *Fundamentals of Spacecraft Attitude Determination and Control*, Springer, 2014.

Prado, I. A. A., Santos, D. A. A Model Predictive Guidance Strategy for a Multirotor Aerial Vehicle, *Journal of Aerospace Technology and Management*, 9, 2017, 116-128.

Santos, D. A., Saotome, O., Cela, A. Trajectory Control of Multirotor Helicopters With Thrust Vector Constraints, *21st Mediterranean Conference on Control and Automation* (MED), 2013, 375-379.

Silva, J. A. B. G., Santos, D. A. Model Predictive Controller Used in Guidance with Obstacle Avoidance of Multirotor Aerial Vehicles, *Congresso Brasileiro de Engenharia Mecânica* (CONEM), Fortaleza, 2016.